Hindawi Publishing Corporation
Journal of Nanomaterials
Volume 2014, Article ID 416765, 7 pages
http://dx.doi.org/10.1155/2014/416765

Research Article

Structural, Optical, and Magnetic Characterization of Spinel Zinc Chromite Nanocrystallines Synthesised by Thermal Treatment Method

Salahudeen A. Gene,[1,2] Elias Saion,[1] Abdul H. Shaari,[1] Mazliana A. Kamarudin,[1] Naif M. Al-Hada,[1] and Alireza Kharazmi[1]

[1] *Department of Physics, Faculty of Science, University Putra Malaysia (UPM), 43400 Serdang, Selangor, Malaysia*
[2] *Department of Physics, Faculty of Applied Science and Technology, Ibrahim Badamasi Babangida University, Lapai 234066, Nigeria*

Correspondence should be addressed to Salahudeen A. Gene; genesalahudeen@gmail.com

Received 18 June 2013; Revised 7 December 2013; Accepted 28 December 2013; Published 5 February 2014

Academic Editor: Claude Estournès

Copyright © 2014 Salahudeen A. Gene et al. This is an open access article distributed under the Creative Commons Attribution License, which permits unrestricted use, distribution, and reproduction in any medium, provided the original work is properly cited.

The present study reports the structural and magnetic characterization of spinel zinc chromite ($ZnCr_2O_4$) nanocrystallines synthesized by thermal treatment method. The samples were calcined at different temperatures in the range of 773 to 973 K. Polyvinylpyrrolidone was used to control the agglomeration of the nanoparticles. The average particle size of the synthesized nanocrystals was determined by powder X-ray diffraction which shows that the crystallite size increases from 19 nm at 773 K to 24 nm at 973 K and the result was in good agreement with the transmission electron microscopy images. The elemental composition of the samples was determined by energy dispersed X-ray spectroscopy which confirmed the presence of Zn, Cr, and O in the final products. Fourier transform infrared spectroscopy also confirmed the presence of metal oxide bands for all the samples calcined at different temperature. The band gap energy was calculated from UV-vis reflectance spectra using the Kubelka-Munk function and the band gap energy of the samples was found to decrease from 4.03 eV at 773 K to 3.89 eV at 973 K. The magnetic properties were also demonstrated by electron spin resonance spectroscopy, the presence of unpaired electrons was confirmed, and the resonant magnetic field and the g-factor of the calcined samples were also studied.

1. Introduction

The spinels are class of minerals of general formulation $A^{2+}B_2{}^{3+}O_4{}^{2-}$ which crystallize in the cubic (isometric) crystal system, with the oxide anions arranged in a cubic close-packed lattice. The cations A and B occupy some or all of the tetrahedral and octahedral sites in the lattice. A and B can be divalent, trivalent, or quadrivalent cations, including magnesium, zinc, iron, manganese, aluminium, chromium, titanium, and silicon. Although the anion is normally oxygen, the analogous thiospinel structure includes the rest of the chalcogenides. Spinels and spinel-like materials are attractive subjects of continuous scientific interest and have been deeply investigated in materials sciences, because of their physical-chemical properties and their wide range of applications as a humidity sensor [1], semiconductors [2], magnetic materials [3], catalysts [4], super hard materials [5], high temperature ceramics [6], among others. In particular, zinc chromite ($ZnCr_2O_4$) ceramic spinels are commonly used as catalytic materials [4], humidity sensors [5], and magnetic material [7].

Various methods have been previously reported on the synthesis of $ZnCr_2O_4$ spinels, which include mechanical activation [8], microemulsion method [9], chemical method [10], microwave method [7], sol-gel method [11], thermal method [12], solution method [13], ultrasonic spray pyrolysis [14], ball milling method [15], and combustion method [16]. Most of the methods are difficult to employ on a large scale production due to the complicated procedures, longer reaction times, high reaction temperatures, toxic reagents,

and by-products involved in these synthesis methods [17]; in this study we have used the thermal treatment method for synthesizing spinel zinc chromite.

The synthesis of spinel $ZnCr_2O_4$ nanocrystals by a thermal treatment method is reported in this study; aqueous solution of only metal nitrates, poly(vinylpyrrolidone), and deionized water was prepared. The solution was dried at 80°C for 24 h, followed by grinding and calcination it at temperatures of the range 773–973 K. This method has the advantages of simplicity, less expense, no unwanted by-products, and being environmentally friendly [18].

In this paper, we have investigated the effect of calcination temperature on the structural, optical, and the magnetic properties of $ZnCr_2O_4$ synthesized by thermal treatment method.

2. Experimental

2.1. Materials. Chromium nitrate $Cr(NO_3)_3{\cdot}9H_2O$ and zinc nitrate $Zn(NO_3)_2{\cdot}6H_2O$ metallic salts were used as metal precursors, polyvinylpyrrolidone (PVP) for controlling the agglomeration of the nanoparticles, and deionized water as solvent. The purchase of $Cr(NO_3)_3{\cdot}9H_2O$ (99%), $Zn(NO_3)_2{\cdot}6H_2O$ (99%), and PVP (MW = 29,000) was from Sigma-Aldrich.

2.2. Methodology. 3 g of PVP was dissolved in 100 mL of deionized water at 343 K, before mixing 0.2 mmol of $Cr(NO_3)_3{\cdot}9H_2O$ and 0.1 mmol of $Zn(NO_3)_2{\cdot}6H_2O$ (Cr : Zn = 2 : 1) into the polymer solution. The solution is constantly stirred until a homogeneous solution is formed. The mixed solution is poured into Petri dish and placed in an oven for 24 h to dry at a temperature of 353 K. The resulting solid was grinded into powder and calcined at temperatures of 773, 823, 873, 923, and 973 K for 3 h.

2.3. Characterization. The structural characterization of the synthesized $ZnCr_2O_4$ nanocrystals was carried out by powder X-ray diffraction (XRD); the morphology and the average particle size were also determined by transmission electron microscopy (TEM). The atomic composition (%) of the constituent elements in the synthesized samples was carried out by energy dispersive X-ray spectroscopy (EDX). Fourier transform infrared spectroscopy (FT-IR) was used to confirm the presence of metallic oxide in the final samples. The optical reflectance spectra were recorded using the UV-vis spectrometer (Shimadz-UV1650PC), and the band gap energy was also evaluated from the reflectance spectra using the Kubelka-Munk function. The magnetic properties were studied using an electron spin resonance spectroscopy (ESR) at room temperature.

3. Results and Discussion

3.1. X-Ray Diffraction Studies. The XRD patterns of samples calcined at different temperatures of 773, 823, 873, 923, and 973 K are shown in Figure 1. The reflection planes of (111), (220), (311), (222), (400), (422), (511), and (440) confirm the presence of $ZnCr_2O_4$ with a face centered cubic structure. The result matches well the phase reported in the powder X-Ray diffraction data base with reference code 01-087-0028 of spinel $ZnCr_2O_4$ crystals in cubic face with a = 8.3267 Å, volume = 577.32 Å, (no. 227). The result shows that the diffraction peaks become sharper and narrower and their intensity increases with increase in calcination temperature. This indicates intensification in crystallinity that originates from the increment of crystalline planes due to the size enlargement of the particles [18]. The average particle size was also determined from the full width of the half maximum (FWHM) peak broadening of the (311) peak of the XRD patterns using Scherrer formula as follows:

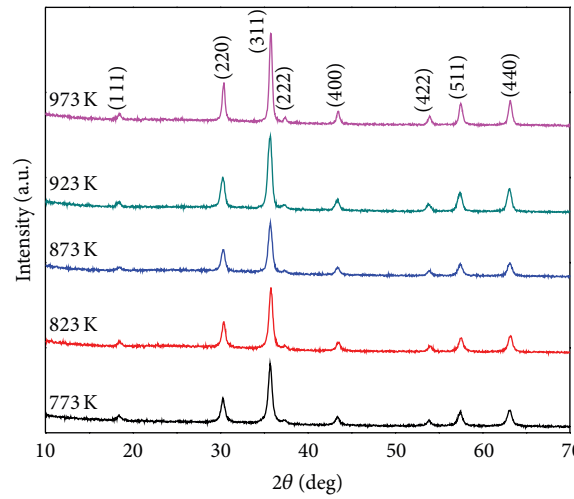

Figure 1: XRD patterns for $ZnCr_2O_4$ powders calcined at temperatures of 773, 823, 873, 923, and 973 K.

$$D = 0.9\left(\frac{\lambda}{\beta}\right)\cos\theta, \tag{1}$$

where D is the crystalline size (nm), β is the full width of the diffraction line at half of the maximum intensity, λ is the X-ray wavelength of Cu Kα = 0.15 nm, and θ is the Bragg angle [19]. The particle sizes estimated using the Scherrer formula were found to increase with the calcination temperature, from about 19 nm at 773 K to about 24 nm at 973 K (Table 1).

3.2. EDX Studies. Figure 2 shows the EDX spectrum of $ZnCr_2O_4$ synthesized by the thermal treatment method. The corresponding peaks of Zn, Cr, and O were observed in the sample which confirms the formation of $ZnCr_2O_4$ and further confirmed the results obtained from XRD analysis. The atomic composition (%) ratios of Zn and Cr were found to be 15.74% and 29.92%, respectively, which match well the amount of Zn and Cr used in the respective precursors. The peaks of Au are originated from the preparation process of the sample for the EDX analysis. Moreover, the thermal treatment method is very effective, because no loss of element occurred in the synthesis process.

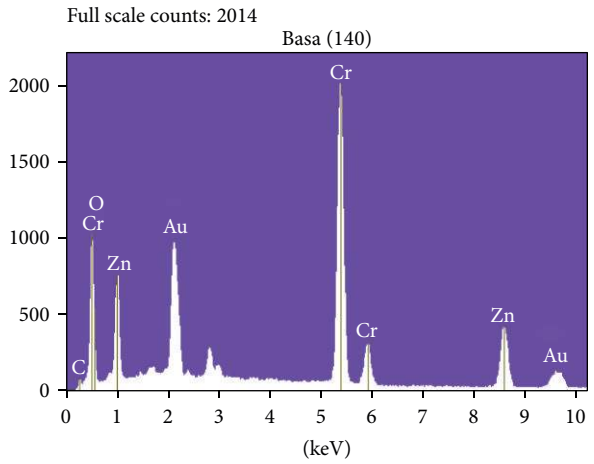

(a)

Element	Measured atom (%)	Normalized	
		Experimental	Theoretical
O	41.13	47.39	57.14
Cr	29.92	34.47	28.57
Zn	15.74	18.14	14.28

(b)

Figure 2: (a) The EDX pattern of calcined sample and (b) the atomic composition of synthesized $ZnCr_2O_4$.

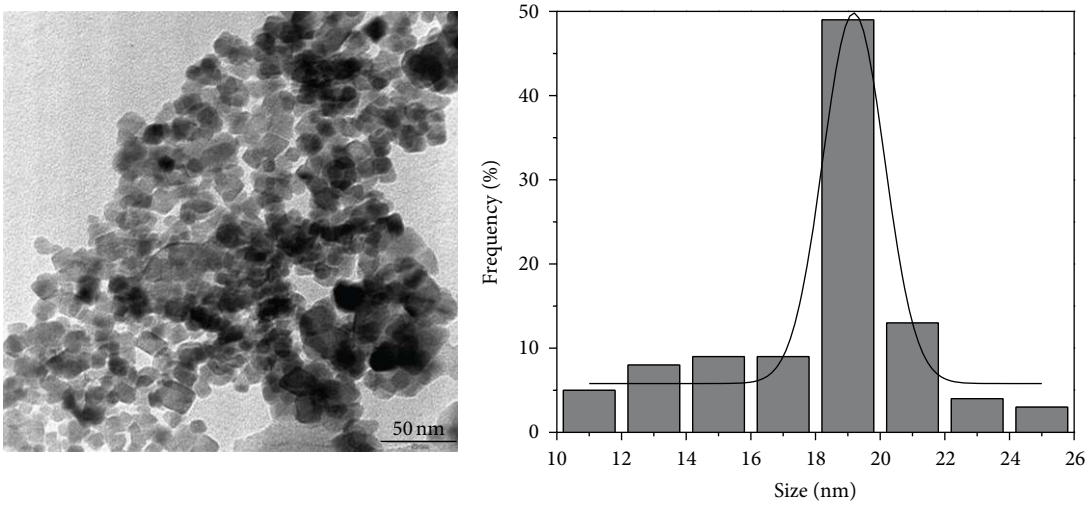

(a)

(b)

Figure 3: TEM image and particle size distribution of samples calcined at (a) 773 K and (b) 973 K.

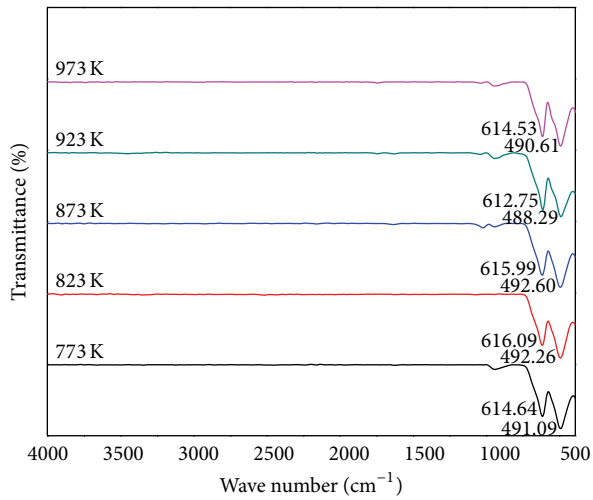

FIGURE 4: The FT-IR spectrum of the calcined samples at temperatures of 773, 823, 873, 923, and 973 K.

3.3. TEM Studies. Figure 3 shows the TEM images and crystal size distribution of $ZnCr_2O_4$ nanocrystallines calcined at (a) 773 and (b) 973 K. The result indicates that the samples prepared by the thermal treatment method were uniform in morphology and particle size distribution. The spinel nanoparticles consist of uniform cubic crystallites with an average size of 19 and 24 nm at temperatures of 773 and 973 K, respectively (Table 1), which are in good agreement with XRD results and also show that the particle size increases with the increase in calcination temperature. This suggested that as the temperature increases, several neighboring particles fused together to increase the particle size by the melting of their surfaces [20].

3.4. FT-IR Spectra Studies. The FT-IR spectrum of the calcined samples at temperature of 773, 823, 873, 923, and 973 K, with the wave number ranging from 380 to 4000 cm^{-1}, is shown in Figure 4. The IR spectra show the two principle absorption bands of Cr–O and Zn–O located at around the range of 490 and 615 cm^{-1}, respectively, for all the calcined samples. These bonds are associated with $ZnCr_2O_4$, and this indicates the formation of spinel $ZnCr_2O_4$ nanocrystals, as suggested by previously published data. These two vibration bands Cr–O and Zn–O corresponded to the intrinsic lattice vibrations of octahedral and tetrahedral coordination compounds in the spinel structure, respectively. The absence of the peaks at 1000–1300 cm^{-1} and 2000–3000 cm^{-1} in the samples confirmed the nonexistence of the O–H mode, C–O mode, and C=H stretching mode of organic sources in the calcined samples [12].

3.5. Optical Properties of $ZnCr_2O_4$ by UV-Visible Reflectance Spectroscopy. The optical diffuse reflectance spectra of $ZnCr_2O_4$ nanocrystals have been recorded using a DR-UV-vis. Figure 5(a) shows the reflectance spectra of the nanocrystals calcined at 773, 823, 873, 923, and 973 K in the wavelength range of 220–650 nm. Two reflection peaks were seen at around 375 nm and 542 nm in samples. The energy band gap of the nanocomposites was determined from the diffuse reflectance spectra using the Kubelka-Munk function by plotting the square of the Kubelka-Munk function $F(R)^2$ versus energy and extrapolating the linear part of the curve to $F(R)^2 = 0$ as shown in samples calcined at temperatures ranging from 773 to 973 K in Figures 5(b)–5(f), respectively; this yields the direct band gap energy of the materials [21]. Optical band gaps of 4.03, 4.00, 3.98, 3.90, and 3.89 eV were obtained for samples calcined at 773, 823, 873, 923, and 973 K, respectively (Table 1); the values of the energy band gaps were found to decrease with increase in calcination temperature. The increase in calcination temperature causes the increase in the particle size and thus, this phenomenon may be attributed to quantum size effect [22].

3.6. Electron Spine Resonance Studies. Figure 6 shows the ESR spectrum of $ZnCr_2O_4$ calcined at 773, 823, 873, 923, and 973 K. Broad and symmetrical signals which are due to the presence of unpaired electrons of the conduction electrons of transition Cr^{3+} ions located in the B-site in the samples were exhibited by all the samples at different temperatures, which indicates that the sample has a paramagnetic property. It is obvious that the values of g-factor increase from 1.9598 to 1.9616 when the calcination temperature increases from 773 to 973 K, respectively (Table 2). This indicates that the internal magnetic field increases with increase in calcination temperature which suggests that microscopic magnetic interactions increase as particle size increases [23].

It was also found that the resonant magnetic field decreases in value from 3.3468×10^{-7} to 3.3437×10^{-7} A/m with an increase in calcination temperature from 773 to 973 K, respectively (Table 2). According to the following equation:

$$g = \frac{h\nu}{\beta H_r}, \tag{2}$$

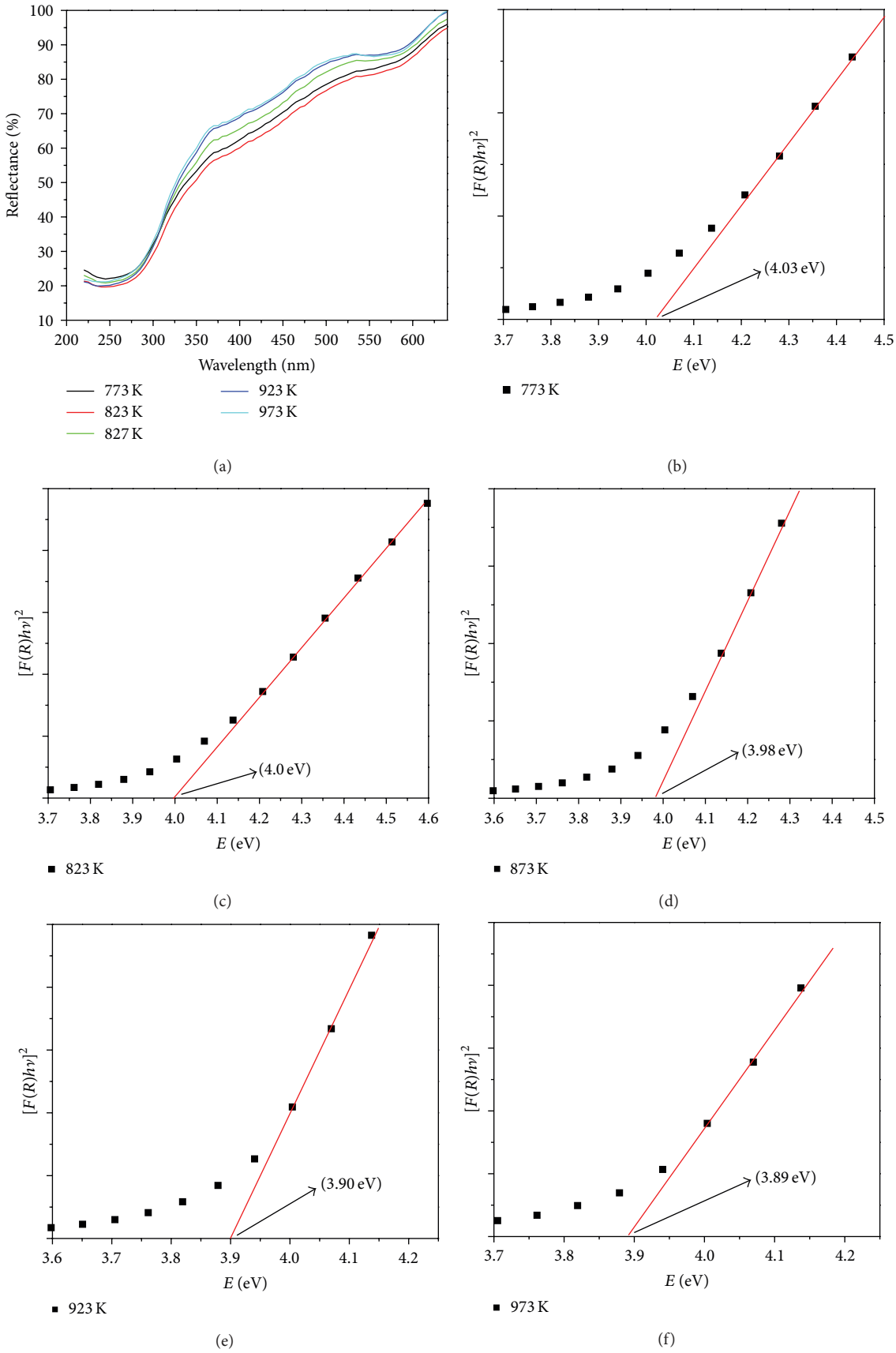

FIGURE 5: (a) Reflectance spectra of the nanocrystals calcined at temperature 773–973 K and plot of the square of Kubelka-Munk function $F(R)^2$ versus energy (b) 773, (c) 823, (d) 873, (e) 923, and (f) 973 K.

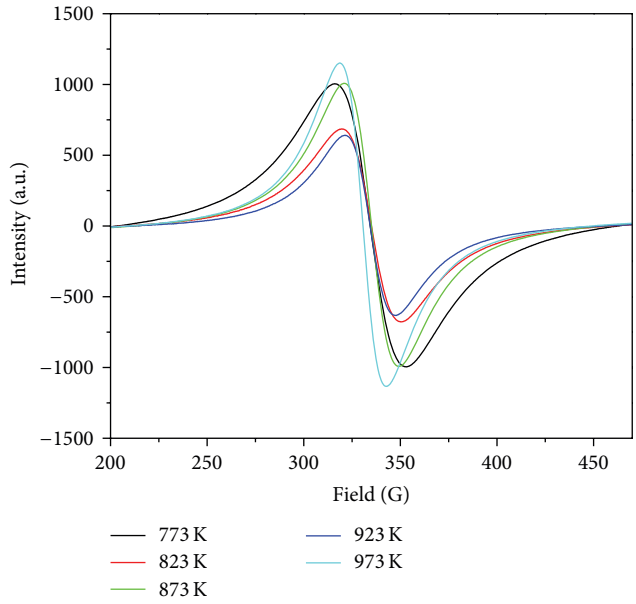

Figure 6: The electron spin resonance spectrum of $ZnCr_2O_4$ calcined at 773, 823, 873, 923, and 973 K.

Table 1: The average particle size of zinc chromite measured by XRD and TEM compared with the band gap energy for samples calcined at 773, 823, 873, 923, and 973 K.

Calcination temperature (K)	Average particle size XRD (nm)	Average particle size TEM (nm) ±2	Band gap energy (eV)
773	19	19	4.03
823	19	20	4.00
873	23	21	3.98
923	23	22	3.90
973	24	24	3.89

Table 2: Magnetic parameters of $ZnCr_2O_4$ observed for ESR analysis.

Calcination temperature (K)	g-factor	Resonance magnetic field (A/M)
773	1.95981	3.34678×10^{-7}
823	1.96123	3.34436×10^{-7}
873	1.96142	3.34404×10^{-7}
923	1.96151	3.34388×10^{-7}
973	1.96156	3.34380×10^{-7}

where h is Planck's constant, ν is the microwave frequency, β is the Bohr magneton (9.274×10^{-24} J·T^{-1}), and H_r is resonant magnetic field, the resonance magnetic field should decrease when g-factor increases, whereas the value of ν is constant in EPR spectroscopy. Increases in g-factor and decreases in H_r with an increase in calcination magnetization values have been reported in previous studies of spinel nanoparticles [24]. In effect, as the crystal size increases with increase in calcination temperature, the Cr^{3+} ions located at the B-site in the structure of the samples cause an increase in the super exchange interaction, which leads to an increase in the internal magnetic field and decrease in the resonance magnetic field of the samples [24, 25].

4. Conclusions

Spinel $ZnCr_2O_4$ nanocrystals were successfully synthesized using the thermal treatment method. Particle sizes ranging from 19 to 24 nm were achieved with calcination temperatures of 773 and 973 K, respectively. The crystal sizes increase with increase in calcination temperature. FT-IR spectroscopy confirmed the existence of metal oxide bands at all calcination temperatures and the peaks of Zn, Cr, and O were observed in the EDX analysis which confirms the formation of $ZnCr_2O_4$. Using the Kubelka-Munk function from UV-vis reflectance spectra, the band gap energy of $ZnCr_2O_4$ was estimated to decrease from 4.03 to 3.89 eV as the calcination temperature increases from 773 to 973 K, respectively. ESR spectroscopy confirmed the existence of unpaired electrons and the resonant magnetic field (H_r) and the g-factor values were also studied. The increases in g-factor and decreases in H_r were observed as the calcination temperature increases from 773 to 973 K which indicates the increase in magnetic properties of the samples as the particle size increases with increase in calcination temperature.

Conflict of Interests

The authors declare that there is no conflict of interests regarding the publishing of this paper.

Acknowledgments

The authors would like to acknowledge the technical supports from the staffs of the Faculty of Science and the Institute of Bioscience (IBS), Universiti Putra Malaysia. This work was financially supported by the Research Management Center (RMC), Universiti Putra Malaysia.

References

[1] M. Bayhan and N. Kavasoğlu, "A study on the humidity sensing properties of $ZnCr_2O_4$–K_2CrO_4 ionic conductive ceramic sensor," *Sensors and Actuators B*, vol. 117, no. 1, pp. 261–265, 2006.

[2] C. L. Honeybourne and R. K. Rasheed, "Nitrogen dioxide and volatile sulfide sensing properties of copper, zinc and nickel chromite," *Journal of Materials Chemistry*, vol. 6, no. 3, pp. 277–283, 1996.

[3] S. Bid and S. K. Pradhan, "Preparation of zinc ferrite by high-energy ball-milling and microstructure characterization by Rietveld's analysis," *Materials Chemistry and Physics*, vol. 82, no. 1, pp. 27–37, 2003.

[4] R. M. Gabr, M. M. Girgis, and A. M. El-Awad, "Formation, conductivity and activity of zinc chromite catalyst," *Materials Chemistry and Physics*, vol. 30, no. 3, pp. 169–177, 1992.

[5] M. Bayhan, T. Hashemi, and A. W. Brinkman, "Sintering and humidity-sensitive behaviour of the $ZnCr_2O_4$–K_2CrO_4 ceramic system," *Journal of Materials Science*, vol. 32, no. 24, pp. 6619–6623, 1997.

[6] D. M. Hulbert, D. Jiang, J. D. Kuntz, Y. Kodera, and A. K. Mukherjee, "A low-temperature high-strain-rate formable nanocrystalline superplastic ceramic," *Scripta Materialia*, vol. 56, no. 12, pp. 1103–1106, 2007.

[7] P. Parhi and V. Manivannan, "Microwave metathetic approach for the synthesis and characterization of $ZnCr_2O_4$," *Journal of the European Ceramic Society*, vol. 28, no. 8, pp. 1665–1670, 2008.

[8] Z. V. Marinković Stanojević, N. Romčević, and B. Stojanović, "Spectroscopic study of spinel $ZnCr_2O_4$ obtained from mechanically activated ZnO–Cr_2O_3 mixtures," *Journal of the European Ceramic Society*, vol. 27, no. 2-3, pp. 903–907, 2007.

[9] X. Niu, W. Du, and W. Du, "Preparation and gas sensing properties of ZnM_2O_4 (M = Fe, Co, Cr)," *Sensors and Actuators B*, vol. 99, no. 2-3, pp. 405–409, 2004.

[10] I. Esparza, M. Paredes, R. Martinez et al., "Solid State reactions in Cr_2O_3-ZnO nanoparticles synthesized by triethanolamine chemical precipitation," *Materials Sciences and Applications*, vol. 2, pp. 1584–1592, 2011.

[11] H. T. Zhang and X. H. Chen, "Synthesis and characterization of nanocrystallite $ZnCrFeO_4$," *Inorganic Chemistry Communications*, vol. 6, no. 8, pp. 992–995, 2003.

[12] M. Stefanescu, M. Barbu, T. Vlase, P. Barvinschi, L. Barbu-Tudoran, and M. Stoia, "Novel low temperature synthesis method for nanocrystalline zinc and magnesium chromites," *Thermochimica Acta*, vol. 526, no. 1-2, pp. 130–136, 2011.

[13] R. G. Chandran and K. C. Patil, "A rapid method to prepare crystalline fine particle chromite powders," *Materials Letters*, vol. 12, no. 6, pp. 437–441, 1992.

[14] Z. V. Marinković, L. Mančić, R. Marić, and O. Milošević, "Preparation of nanostructured Zn–Cr–O spinel powders by ultrasonic spray pyrolysis," *Journal of the European Ceramic Society*, vol. 21, pp. 2051–2055, 2001.

[15] Z. V. Marinković, L. Mančić, P. Vulić, and O. Milošević, "Microstructural characterization of mechanically activated ZnO–Cr_2O_3 system," *Journal of the European Ceramic Society*, vol. 25, pp. 2081–2084, 2005.

[16] S. V. Bangale and S. R. Bamane, "Preparation, wetability and electrical properties of nanocrystalline $ZnCr_2O_4$ oxide by combustion route," *Archives of Applied Science Research*, vol. 3, pp. 300–308, 2011.

[17] M. G. Naseri, E. B. Saion, and A. Kamali, "An overview on nanocrystalline $ZnFe_2O_4$, $MnFe_2O_4$, and $CoFe_2O_4$ synthesized by a thermal treatment method," *ISRN Nanotechnology*, vol. 2012, Article ID 604241, 11 pages, 2012.

[18] M. G. Naseri, E. B. Saion, H. A. Ahangar, A. H. Shaari, and M. Hashim, "Simple synthesis and characterization of cobalt ferrite nanoparticles by a thermal treatment method," *Journal of Nanomaterials*, vol. 2010, Article ID 907686, 8 pages, 2010.

[19] B. D. Cullity, *Elements of X Ray Diffraction*, BiblioBazaar, 2011.

[20] Y. Qu, H. Yang, N. Yang, Y. Fan, H. Zhu, and G. Zou, "The effect of reaction temperature on the particle size, structure and magnetic properties of coprecipitated $CoFe_2O_4$ nanoparticles," *Materials Letters*, vol. 60, no. 29-30, pp. 3548–3552, 2006.

[21] G. Kortüm and J. E. Lohr, *Reflectance Spectroscopy: Principles, Methods, Applications*, Springer, London, UK, 2012.

[22] A. Manikandan, J. J. Vijaya, L. J. Kennedy, and M. Bououdina, "Structural, optical and magnetic properties of $Zn_{1-x}Cu_xFe_2O_4$ nanoparticles prepared by microwave combustion method," *Journal of Molecular Structure*, vol. 1035, pp. 332–340, 2013.

[23] G. Vaidyanathan and S. Sendhilnathan, "Characterization of $Co_{1-x}Zn_xFe_2O_4$ nanoparticles synthesized by co-precipitation method," *Physica B*, vol. 403, no. 13-16, pp. 2157–2167, 2008.

[24] M. G. Naseri, E. B. Saion, H. A. Ahangar, and A. H. Shaari, "Fabrication, characterization, and magnetic properties of copper ferrite nanoparticles prepared by a simple, thermal-treatment method," *Materials Research Bulletin*, vol. 48, pp. 1439–1446, 2013.

[25] P. Priyadharsini, A. Pradeep, P. S. Rao, and G. Chandrasekaran, "Structural, spectroscopic and magnetic study of nanocrystalline Ni-Zn ferrites," *Materials Chemistry and Physics*, vol. 116, no. 1, pp. 207–213, 2009.

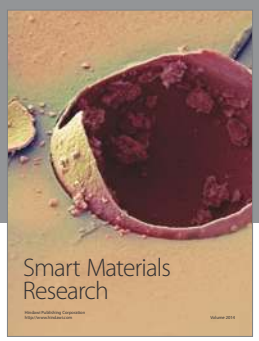

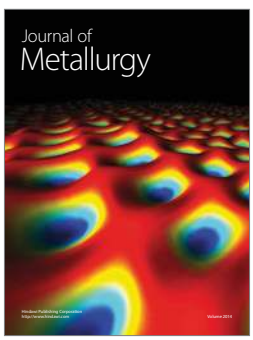

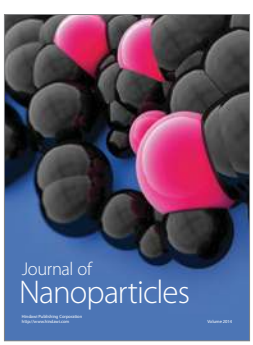

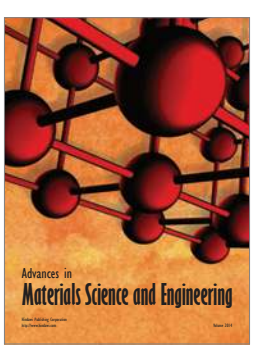

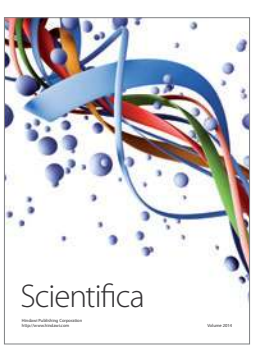

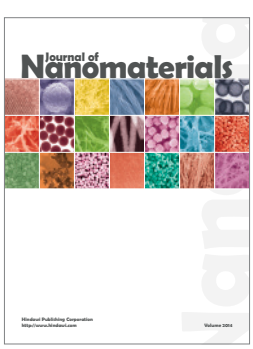

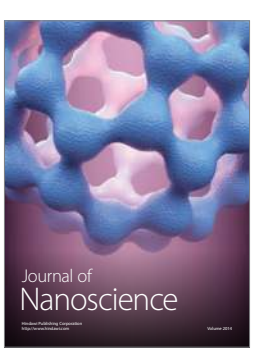

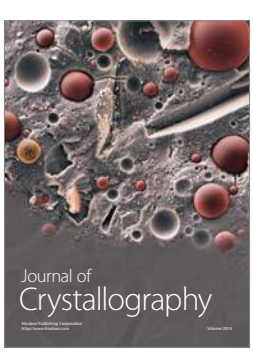

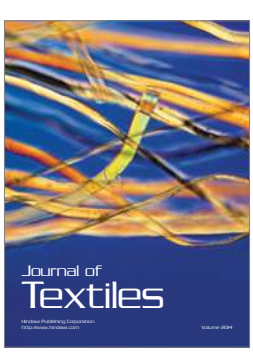

Hindawi

Submit your manuscripts at
http://www.hindawi.com